BMC Medical Imaging

RESEARCH

Open Access

A prior information-based multi-population multi-objective optimization for estimating ^{18}F-FDG PET/CT pharmacokinetics of hepatocellular carcinoma

Yiwei Xiong[1], Siming Li[1], Jianfeng He[1,3*] and Shaobo Wang[2*]

Abstract

Background ^{18}F fluoro-D-glucose (^{18}F-FDG) positron emission tomography/computed tomography (PET/CT) pharmacokinetics is an approach for efficiently quantifying perfusion and metabolic processes in the liver, but the conventional single-individual optimization algorithms and single-population optimization algorithms have difficulty obtaining reasonable physiological characteristics from estimated parameters. A prior-based multi-population multi-objective optimization (p-MPMOO) approach using two sub-populations based on two categories of prior information was preliminarily proposed for estimating the ^{18}F-FDG PET/CT pharmacokinetics of patients with hepatocellular carcinoma.

Methods PET data from 24 hepatocellular carcinoma (HCC) tumors of 5-min dynamic PET/CT supplemented with 1-min static PET at 60 min were prospectively collected. A reversible double-input three-compartment model and kinetic parameters (K_1, k_2, k_3, k_4, f_a, and v_b) were used to quantify the metabolic information. The single-individual Levenberg–Marquardt (LM) algorithm, single-population algorithms (Particle Swarm Optimization (PSO), Differential Evolution (DE), and Genetic Algorithm (GA)) and p-MPMO optimization algorithms (p-MPMOPSO, p-MPMODE, and p-MPMOGA) were used to estimate the parameters.

Results The areas under the curve (AUCs) of the three p-MPMO methods were significantly higher than other methods in K_1 and k_4 ($P<0.05$ in the DeLong test) and the single population optimization in k_2 and k_3 ($P<0.05$), and did not differ from other methods in f_a and v_b ($P>0.05$). Compared with single-population optimization, the three p-MPMO methods improved the significant differences between K_1, k_2, k_3, and k_4. The p-MPMOPSO showed significant differences ($P<0.05$) in the parameter estimation of k_2, k_3, k_4, and f_a. The p-MPMODE is implemented on K_1, k_2, k_3, k_4, and f_a; The p-MPMOGA does it on all six parameters.

Conclusions The p-MPMOO approach proposed in this paper performs well for distinguishing HCC tumors from normal liver tissue.

*Correspondence:
Jianfeng He
jfenghe@foxmail.com
Shaobo Wang
wshbo_98@126.com

Full list of author information is available at the end of the article

Keywords ^{18}F FDG PET/CT, Prior information, Multi-population multi-objective optimization

Introduction

Dynamic ^{18}F-FDG PET/CT has been widely applied in clinical studies for liver cancer diagnosis. Using tracer kinetic modeling (TKM) of time-activity curve (TAC) data, the HCC can be diagnosed according to quantified physiological information [1].

Pharmacokinetic-based compartmental modeling stands as a widely utilized approach for acquiring quantitative information on tracer metabolism within biological tissues [2, 3]. Sokoloff et al. [4] proposed an irreversible three-compartment model with the parameters K_1, k_2 and k_3. Graham et al. [5] investigated the effect of the parameter k_4, and the results indicated that neglecting the dephosphorylation process led to modeling bias. Given the dual blood supply characteristics of the liver, utilizing the dual blood input from the hepatic artery and portal vein has emerged as the optimal approach for hepatic kinetic modeling [6, 7]. In addition, image-derived blood input acquisition has replaced blood sampling as a result of its noninvasiveness [8].

Simultaneous extraction of plasma TAC and tissue TAC data serves as the basis for kinetic modeling, allowing the derivation of physiological information through parameter estimation. The nonlinear least squares (NLLS) method is commonly used for parameter estimation. In previous studies, single-individual optimization algorithms such as the Levenberg–Marquardt (LM) algorithm [9], which is generally considered prone to convergence to local optima [10–13], have been applied. Moreover, metaheuristic-based population optimization algorithms such as PSO [14], DE [15], and GA [16] perform well in global optimization. Nevertheless, challenges persist in ensuring that these parametric solutions accurately represent physiological processes. Although studies employing population optimization have shown the potential of achieving smaller fitting errors, these parameters might unexpectedly fall outside the anticipated range, thereby adversely affecting diagnostic outcomes. In one study, the identifiability of the three-compartment model was analyzed, revealing the possibility of multiple local solutions within the solution space and implying that modeling and solving of TAC data may be more challenging in practice than theoretically anticipated [10]. Thus, estimating parameters based on finding the solution with the smallest error may not truly reflect physiological characteristics, potentially leading to non-significant statistical differences in the parameter results [17, 18]. Applying prior information is one solution, and straightforward alternatives include setting physiologically reasonable fixed boundaries for the parameters [19] or using a specific reliable value to determine a certain kinetic parameter [20]; however, the actual parameter may not almost conform to these fixed restriction rules. He et al. [13] combined prior knowledge to the Bayesian method and obtained reliable parameters. Lin et al. [21] used prior information to guide the optimization process for parametric imaging of hybrid models, obtaining more stable results in terms of the Cramér–Rao lower bounds metric. Ghovvati et al. [22] used a penalty function in a hybrid GA and PSO algorithm to avoid infeasible points. Kanga et al. [23] used PSO for infinity-norm regularization-based parameter estimation of three-compartment models and used prior information to accelerate the optimization process. However, the utilization of prior information within population optimization algorithms has not been extensively explored in the literature. In this work, we innovatively integrated prior information into the framework of population optimization algorithms, aiming to enhance the physiological rationality of parameter estimation outcomes in the dynamic ^{18}F-FDG PET/CT pharmacokinetic modeling.

Materials and methods

Dynamic PET/CT data (patient characteristics)

This study received approval from the Institutional Review Committee of the First People's Hospital of Yunnan Province (No. KHLL2022-KY189). The patients all underwent 5-min short-term dynamic ^{18}F-FDG PET/CT scans and 1-min whole-body conventional static scans prior to receiving any treatment. Twenty-one patients, all of whom had confirmed diagnoses of HCC, participated in the study, contributing data. Among the patients, there were 20 males and 1 female, with ages ranging from 31 to 78 years. Nineteen patients had one tumor, one patient had two tumors, and one patient had three tumors, resulting in a total of 24 pathologically diagnosed HCC tumors. These tumors varied in size, with the long axis ranging from 1.9 to 15.0 cm (mean 6.5 ± 3.6). In terms of differentiation grade, 7 tumors were classified as well-differentiated, 10 as moderately differentiated, and 7 as poorly differentiated. Informed consent was acquired from all patients, and all methods adhered to the principles outlined in the Declaration of Helsinki.

PET imaging was performed using a Philips Ingenuity TF PET/CT scanner (Cleveland, OH, USA), while Philips IntelliSpace Portal v7.0.4.20175 was used for imaging post-processing. ^{18}F-FDG synthesis was carried out using a chemical synthesis module (PET Biotechnology Co., Ltd., Beijing, China), ensuring a radiochemical purity exceeded 95%. The PET/CT scanning procedure for each patient was as follows: at least 6 h of fasting before injection and a bedside low-dose liver CT scan (120 kV, 100

mAs) for attenuation correction and image fusion was performed; ^{18}F-FDG injection was then performed, followed by rapid manual application of ^{18}F-FDG (5.5 MBq/kg) in 2 mL of 0.9% saline and at a 2 mL/s. The flow was flushed with 2 mL of 0.9% saline, and after injection into the vein, a 5-min dynamic PET scan was performed. To observe the time course of tracer uptake, the PET axial field of view was centered on the liver during the scan; Subsequently, a conventional static PET scan was conducted around the 60th minute after the injection, complemented by whole-body CT scans spanning from the apex of the skull to the proximal thighs (120 kV, 200 mAs). Following the CT scans, a 1-min PET scan was conducted at each scanning position. Twelve frames of 5s and four frames of 60s were reconstructed from the 5-min dynamic PET data. In addition, one frame of static PET scan data at 60 min to form a total of 17 frames of PET data. The reconstruction algorithm employed adhered to the standard ordered subsets expectation maximization (OSEM).

Regions of interest (ROIs) of the artery, portal vein, HCC, and background liver tissues, were primarily manually drawn on PET images or CT images and adjusted slice-by-slice. When the delineation was challenging, CT images were used as an aid to refine the boundaries. For arteries and portal veins, ROIs were drawn to cover approximately two-thirds of the vascular cross-section, ensuring the exclusion of adjacent structures. For HCC tumors and normal liver tissues, blood vessels were carefully excluded from the ROIs to avoid interference. The maximum standardized uptake values (SUVmax) were extracted from each frame of the PET/CT images in the ROIs and comprised the time-activity curves (TACs) of the tissues.

Kinetic modeling

The compartmental model used in this paper is the reversible (k4≥0) double-input three-compartment model (r-DI-3CM) [24], as shown in Fig. 1.

$C_a(t)$ is the hepatic arterial input concentration, $C_v(t)$ is the portal vein input concentration. The total model input function (the blood tracer concentration $C_i(t)$) is obtained by weighted summation of the two blood input functions according to the hepatic artery blood supply fraction (f_a):

$$C_i(t) = f_a \times C_a(t) + (1 - f_a) \times C_v(t) \quad (1)$$

$C_f(t)$ and $C_p(t)$ represent the tracer concentrations of the free ^{18}F-FDG compartment and phosphorylated FDG compartment, respectively. The kinetic parameter K_1 (ml/min/ml) in the figure represents the rate constant of ^{18}F-FDG transport from the blood to the hepatocyte, k_2 (1/min) is the clearance rate of ^{18}F-FDG transport back to the blood, k_3 represents the rate constant of phosphorylation of ^{18}F-FDG to ^{18}F-FDG-6-phosphate, and k_4 represents the dephosphorylation rate of phosphatase.

The pharmacokinetic process of r-DI-3CM can be modeled by the following ordinary differential equations:

$$\frac{d}{dt}C(t) = M \cdot C(t) + k_1 C_i(t) \cdot e, \quad C(0) = 0 \quad (2)$$

$$M = \begin{bmatrix} -(k_2+k_3) & k_4 \\ k_3 & -k_4 \end{bmatrix}, \quad C = \begin{bmatrix} C_f \\ C_p \end{bmatrix}, \quad e = \begin{bmatrix} 1 \\ 0 \end{bmatrix} \quad (3)$$

where t is time, and $C(t)$ is the total output tracer concentration function, the expression of the concentration function is $[c(t_1), c(t_2), \cdots, c(t_k)]^T$, and k is the total number of PET scanning protocol frames. The matrix form of the system of equations is as follows:

$$\begin{bmatrix} \frac{d}{dt}C_f(t) \\ \frac{d}{dt}C_p(t) \end{bmatrix} = \begin{bmatrix} -(k_2+k_3) & k_4 \\ k_3 & -k_4 \end{bmatrix} \times \begin{bmatrix} C_f(t) \\ C_p(t) \end{bmatrix} + \begin{bmatrix} K_1 C_i(t) \\ 0 \end{bmatrix} \quad (4)$$

The ordinary differential equation is solved to obtain:

$$C(t; k, C_i) = k_1 \int_0^t e^{M \cdot (t-\tau)} \cdot C_i(\tau)\, e d\tau \quad (5)$$

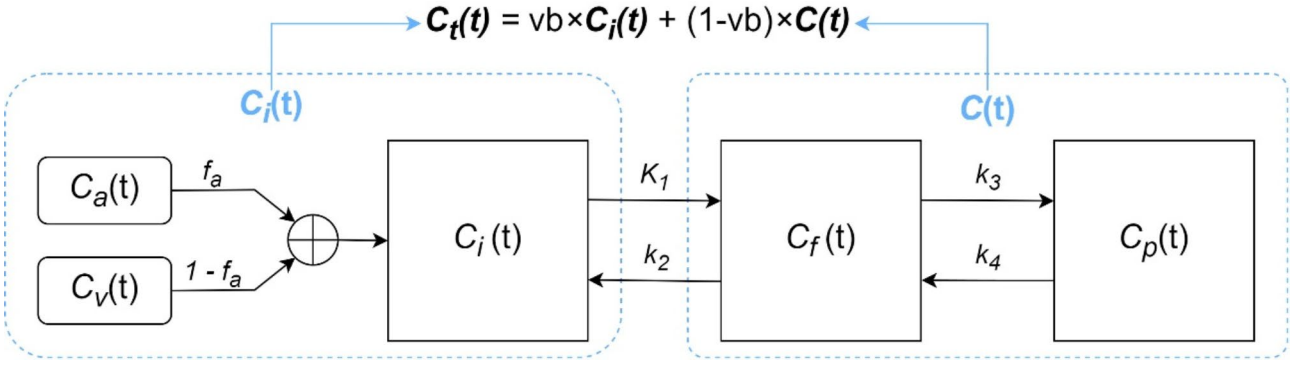

Fig. 1 Double-input reversible three-compartment model (DI-3CM)

The compartmental model also includes the parameter v_b, which is the fractional blood volume. The tissue concentration is calculated by the following equation with v_b :

$$C_t(t) = v_b \times C_i(t) + (1 - v_b) \times C(t) \tag{6}$$

where $C_t(t)$ is the total concentration, $C_i(t)$ is the blood input concentration; and $C(t) = C_f(t) + C_p(t)$ is the tissue concentration.

Prior-based multi-population optimization algorithm

In this paper, we propose to introduce physiological information from prior kinetic parameters into the population optimization process. As a crucial element of the proposed approach, the prior information is obtained through parameter estimation on true TAC data and conducting probability statistics, and the final representation is a statistical distribution over each parameter dimension. The prior parameter samples should be categorized into two groups ("normal" and "tumor") based on the diagnostic classification of the corresponding TACs. As illustrated in Fig. 2, the proposed p-MPMO optimization delineates two independent subpopulations, highlighted by the blue dotted lines in the figure, wherein independent population optimization is conducted. The actual optimization algorithm applied within the two subpopulations can be freely chosen. According to the differences in the statistical distributions of the kinetic parameters between the "normal" and "tumor" categories of the TAC data, two distinctions between optimizations of subpopulations are: First, the parameters of individuals in the subpopulations are initialized with different probabilities of prior information, enabling each subpopulation to present its category's prior probability distribution. Second, the objective function of the optimization applied within the subpopulation differs. The method involved utilizing the corresponding category's prior information to perform a weighted sum multi-objective optimization, with the two objectives being the root-mean-square error (RMSE) between the measured and fitted curves and the prior probability scores. After both subpopulations were optimized, a classification judgment was performed to select one of the results as the final result, where RMSE was used as a metric for judgment.

In the p-MPMO optimization, each subpopulation performed a multi-objective optimization of the RMSE objective and the prior probability scores, and a weighted sum of the two objectives formed a prior weighted objective function. The probability values in the prior information statistical distribution (histogram distribution in this work) of each parameter solution were p_{K_1}, p_{k_2}, p_{k_3}, p_{k_4}, p_{f_a} and p_{v_b}. The values were normalized by a [0, 1] normal distribution, and a weighted sum was used to to obtain the prior probability score s_p:

$$s_p = \sum\nolimits_i w_i \times \frac{p_i - \mu_i}{\sigma_i} \tag{7}$$

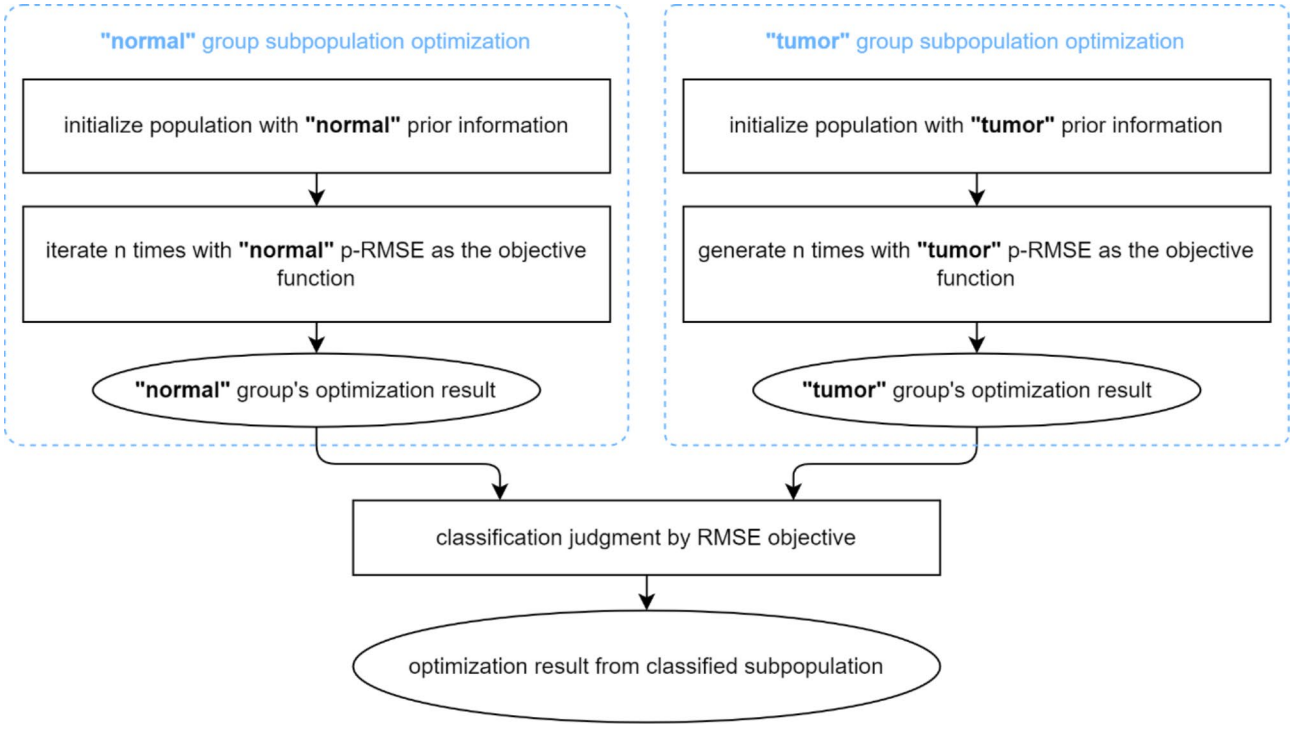

Fig. 2 Flow chart of p-MPMO optimization approach

where μ_i and σ_i were the probability mean and standard deviation, respectively, in the prior distribution of the i th kinetic parameter, and w_i represented the prior probability weights set for the i th kinetic parameter. Finally, the prior weighted RMSE

$$pRMSE = RMSE - s_p \tag{8}$$

is defined as the actual objective function in each subpopulation optimization.

Parameter estimation and metrics

The optimization algorithm and parameter estimation were implemented using Python 3.8. Statistical analyses and Receiver Operating Characteristic (ROC) analyses were performed using scipy 1.6.2 and sklearn 0.24.1.

The results of parameter estimation were evaluated from the aspects of fitting effect, physiological characteristics, and diagnostic significance. RMSE and the fitting curves were used to objectively and subjectively assess the fitting effect of the parameter estimates, respectively; The mean and standard deviation of the parameter estimation were used to present the quantified physiological characteristics of the parameters. Student's t-test was used to test for statistical differences between HCCs and background liver tissue ($p<0.05$) is considered statistically significant), i.e., the diagnostic significance of the parameters.

Results

Prior information acquisition

First, this study used the single-population GA to estimate the parameters and generate prior information. The source data from 24 cases were used to perform twenty parameter estimations for kinetic modeling, and the results were presented as the statistical histogram distribution shown in Fig. 3:

The difference between the statistical distributions of HCC and normal liver tissues in Fig. 3. is significant, and the parameter values are in the correct range and magnitude relationship, i.e., presenting a physiological rationality of the kinetic parameters.

Parameter estimation and statistical analysis

This section demonstrates the fitting effects and statistically significant differences among the kinetic parameters estimated by the p-MPMOPSO, p-MPMODE, and p-MPMOGA. The average value of all repeated parameter estimations was used as the final result for each parameter, and the mean and standard deviation were obtained from the sample of all cases' parameter results. The results are compared with those of the corresponding single-population algorithm as well as the single-individual LM algorithm. The kinetic parameters results of all methods are shown below.

Table 1 shows the results of the single-individual LM optimization algorithm. Since the optimization of the LM algorithm is very sensitive to the initial parameter points, ten repetitions were performed, and the initial parameter values for each optimization were randomly valued within the upper and lower bounds. The LM algorithm showed statistically significant differences among the parameters k_2, k_3, and f_a ($p<0.05$) between HCC tumors and healthy liver tissue, while it did not among the K_1, k_4, and v_b.

Three population optimization algorithms PSO, DE, and GA, and that of their prior-based multi-population optimization algorithms were compared. For the single-population algorithms, the number of individuals was 100, and the number of iterations was 20. However, for the multi-population methods, each subpopulation included 60 individuals, and the number of iterations was 12 because two sub-populations were considered. As for the prior probability weights, all p-MPMO methods used a setting of $w = [0.08,0.02,0.06,0.03,0.05,0.02]$.

Table 2 shows a comparison of the results obtained by the SPPSO and p-MPMOPSO. The SPPSO showed statistically significant differences in k_4 and f_a ($p<0.05$), while it did not in the other four parameters. In comparison, the p-MPMOPSO had lower p values for k_2, k_4, and f_a ($p<0.001$). Furthermore, the statistical distribution of K_1 values is larger in HCC compared to normal liver tissue, which indicates the correct characterization of the pharmacokinetics process, however, that is not presented in the results of SPPSO.

Table 3 shows a comparison of the results obtained by the SPDE and p-MPMODE. The SPDE showed statistically significant differences in k_2, k_4, and f_a ($p<0.05$), while the p-MPMODE showed significant differences in K_1, k_2, k_3, k_4, and f_a.

Table 4 shows a comparison of the SPGA and p-MPMOGA results. The SPGA made three parameters (k_2, k_4, and f_a) showed statistically significant differences, while the p-MPMOGA did that among all parameters.

ROC analysis

As shown in Fig. 4, the three p-MPMO optimization algorithms (blue line) had higher AUC values than the corresponding single population algorithms (orange line) on most parameters.

To determine whether the diagnostic performance of the parameter from one algorithm was significantly better than the others, the following DeLong tests [25] were performed.

The results in Fig. 5; Table 5 indicated that: In K_1 and k_4, the three p-MPMO optimization algorithms

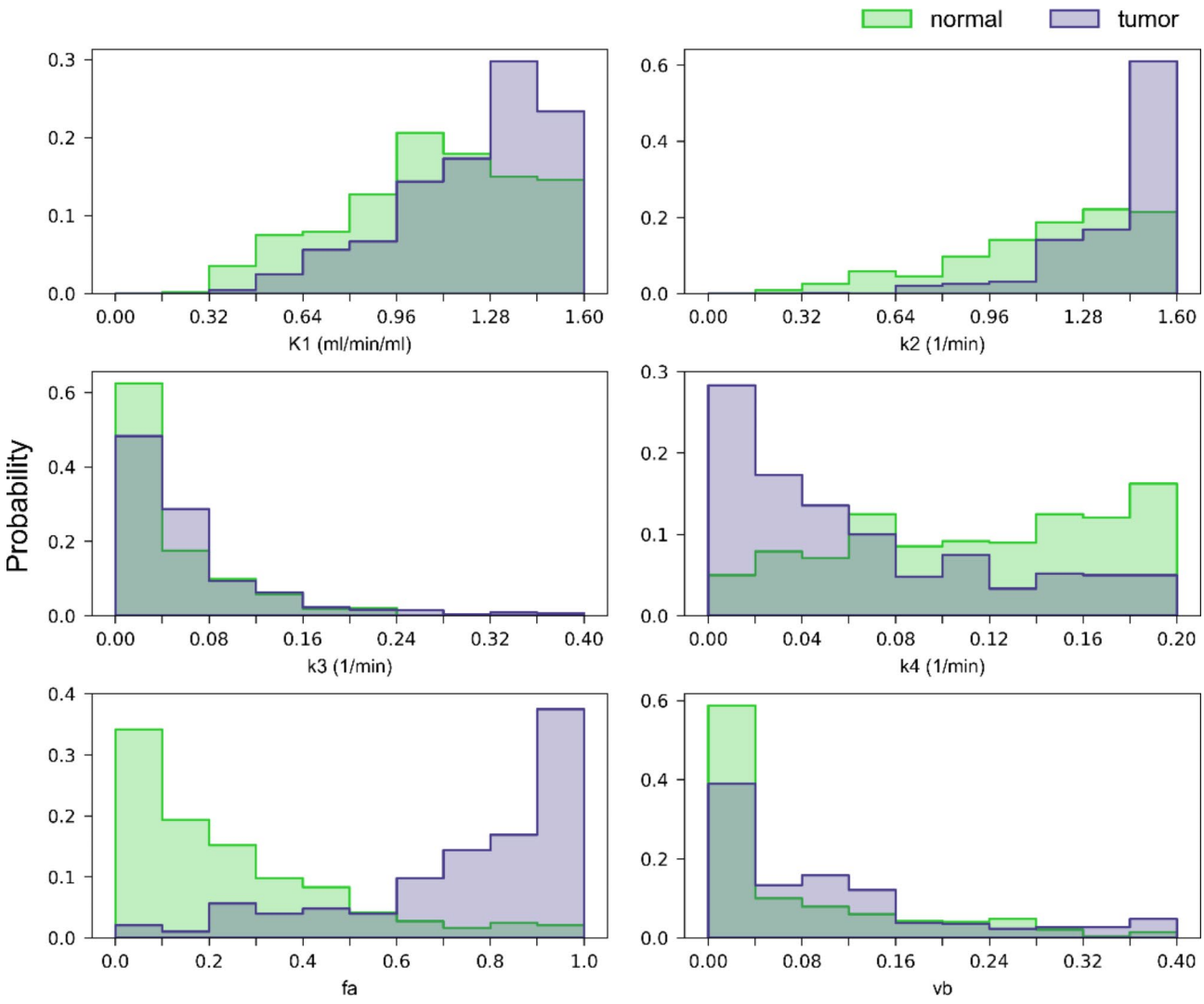

Fig. 3 Prior kinetic parameters histogram distribution

Table 1 The parameters estimation and statistically significant differences by LM

Parameters or metric	Normal	Tumor	*P* value
K_1 (ml/min/ml)	1.242 ± 0.394	1.247 ± 0.259	0.956
k_2 (1/min)	1.247 ± 0.393	1.480 ± 0.200	0.013
k_3 (1/min)	0.006 ± 0.011	0.041 ± 0.079	0.036
k_4 (1/min)	0.104 ± 0.077	0.099 ± 0.089	0.839
f_a	0.233 ± 0.224	0.853 ± 0.244	**< 0.001**
v_b	0.046 ± 0.078	0.074 ± 0.095	0.264
RMSE	1.032 ± 1.004	1.226 ± 0.615	

achieved significantly better diagnostic performance than the corresponding single population algorithms and the LM algorithm. In k_2 and k_3, the three p-MPMO methods were better than the corresponding single population algorithms. However, compared with the LM algorithm in k_2, the p-MPMOPSO was significantly better, the p-MPMOGA was no significant difference, and the p-MPMODE was significantly worse. Moreover, compared with the LM algorithm in k_2, the three p-MPMO optimization algorithms were significantly worse. In f_a and v_b, there was no statistically significant difference in diagnostic performance among the seven algorithms, except that p-MPMODE and p-MPMOGA were significantly worse than that of the LM algorithm in f_a.

TAC curve fitting

Figure 5 demonstrates the comparison of TAC curve fitted by the SPPSO, SPDE, SPGA, p-MPMOPSO, p-MPMODE, and p-MPMOGA. The LM algorithm was not included due to it being a single individual optimization algorithm. The agreement between the measured data (started point) and the fitted data curve represents the fitting effect. The 60 min point was not shown due to it being too far from the previous point at 5 min. As

Table 2 The parameters estimation and statistically significant differences by SPPSO and p-MPMOPSO

Parameters or metric	SPPSO			*p*-MPMOPSO		
	Normal	Tumor	*P* value	Normal	Tumor	*P* value
K_1 (ml/min/ml)	1.176 ± 0.286	1.163 ± 0.206	0.856	1.169 ± 0.253	1.282 ± 0.179	0.080
k_2 (1/min)	1.222 ± 0.280	1.339 ± 0.197	0.103	1.226 ± 0.261	1.469 ± 0.140	**< 0.001**
k_3 (1/min)	0.049 ± 0.041	0.057 ± 0.039	0.458	0.033 ± 0.031	0.053 ± 0.036	0.054
k_4 (1/min)	0.110 ± 0.021	0.100 ± 0.031	0.196	0.115 ± 0.032	0.082 ± 0.047	0.006
f_a	0.256 ± 0.191	0.758 ± 0.184	**< 0.001**	0.218 ± 0.210	0.731 ± 0.231	**< 0.001**
v_b	0.060 ± 0.047	0.106 ± 0.091	0.031	0.064 ± 0.058	0.104 ± 0.096	0.094
RMSE	1.312 ± 1.184	1.580 ± 0.834		1.168 ± 0.996	1.475 ± 0.701	

Table 3 The parameters estimation and statistically significant differences by SPDE and p-MPMODE

Parameters or metric	SPDE			*p*-MPMODE		
	Normal	Tumor	*P* value	Normal	Tumor	*P* value
K_1 (ml/min/ml)	1.091 ± 0.274	1.174 ± 0.206	0.242	1.061 ± 0.234	1.195 ± 0.210	0.043
k_2 (1/min)	1.221 ± 0.263	1.311 ± 0.099	0.119	1.128 ± 0.223	1.311 ± 0.108	0.001
k_3 (1/min)	0.088 ± 0.048	0.072 ± 0.037	0.219	0.050 ± 0.023	0.078 ± 0.051	0.018
k_4 (1/min)	0.115 ± 0.020	0.121 ± 0.020	0.325	0.121 ± 0.033	0.082 ± 0.039	**< 0.001**
f_a	0.249 ± 0.193	0.727 ± 0.155	**< 0.001**	0.253 ± 0.203	0.681 ± 0.177	**< 0.001**
v_b	0.080 ± 0.058	0.116 ± 0.082	0.086	0.093 ± 0.046	0.124 ± 0.080	0.107
RMSE	1.295 ± 1.103	1.706 ± 0.861		1.446 ± 1.111	1.892 ± 0.858	

Table 4 The parameters estimation and statistically significant differences by SPGA and p-MPMOGA

Parameters or metric	SPGA			*p*-MPMOGA		
	Normal	Tumor	*P* value	Normal	Tumor	*P* value
K_1 (ml/min/ml)	1.034 ± 0.244	1.182 ± 0.220	0.032	1.092 ± 0.206	1.242 ± 0.193	0.013
k_2 (1/min)	1.172 ± 0.217	1.329 ± 0.114	0.003	1.168 ± 0.232	1.373 ± 0.106	**< 0.001**
k_3 (1/min)	0.101 ± 0.058	0.082 ± 0.038	0.184	0.029 ± 0.016	0.053 ± 0.050	0.029
k_4 (1/min)	0.112 ± 0.027	0.109 ± 0.026	0.727	0.124 ± 0.023	0.077 ± 0.045	**< 0.001**
f_a	0.246 ± 0.189	0.697 ± 0.189	**< 0.001**	0.239 ± 0.205	0.698 ± 0.221	**< 0.001**
v_b	0.091 ± 0.059	0.137 ± 0.082	0.030	0.076 ± 0.047	0.123 ± 0.091	0.031
RMSE	1.397 ± 1.177	1.797 ± 0.861		1.302 ± 1.046	1.623 ± 0.676	

shown, the three p-MPMO optimization algorithms showed ideal agreement with the original curve data.

Discussion

In this work, kinetic parameters were estimated within the reversible double-input three-compartment model based on PET TAC data, and the hepatic physiological information is presented for the diagnostic study of HCC. The primary objective of this study was to introduce an enhanced approach that offers a more precise quantification and qualification of this information, which may be difficult due to the incorrect physiological characteristics of the kinetic parameters result. Our findings demonstrate that the incorporation of prior information into multi-population optimization algorithms may help parameter estimation more representative of reasonable pharmacokinetic activity. In the results, the p-MPMOPSO, p-MPMODE, and p-MPMOGA demonstrated statistical differences in parameters between normal liver and HCC TACs. The individuals in the population tend to conform to the statistical distribution of the physiological characteristic after applying the prior information, without completely negating the potential of other locations in the solution space.

In this work, a scanning protocol that 5-min dynamic PET supplemented by 1-min static PET at 60 min post-injection [26, 27] was used, and this scheme could maintain a reliable signal-to-noise ratio compared to the scheme that uses a shorter scan interval [28, 29]. The image ROI-derived input function acquisition method was used to obtain hepatic artery and portal vein blood input functions, which is more patient-friendly and easier to perform compared to invasive blood sampling methods [30].

Intelligent population optimization algorithms are a category of optimization algorithms that are gaining popularity across diverse fields. These algorithms have more powerful high-dimensional global optimization capabilities than the single-individual optimization algorithms employed in previous studies. Several studies have utilized the computational advantages to reduce fitting errors. However, in practice, certain positions within the

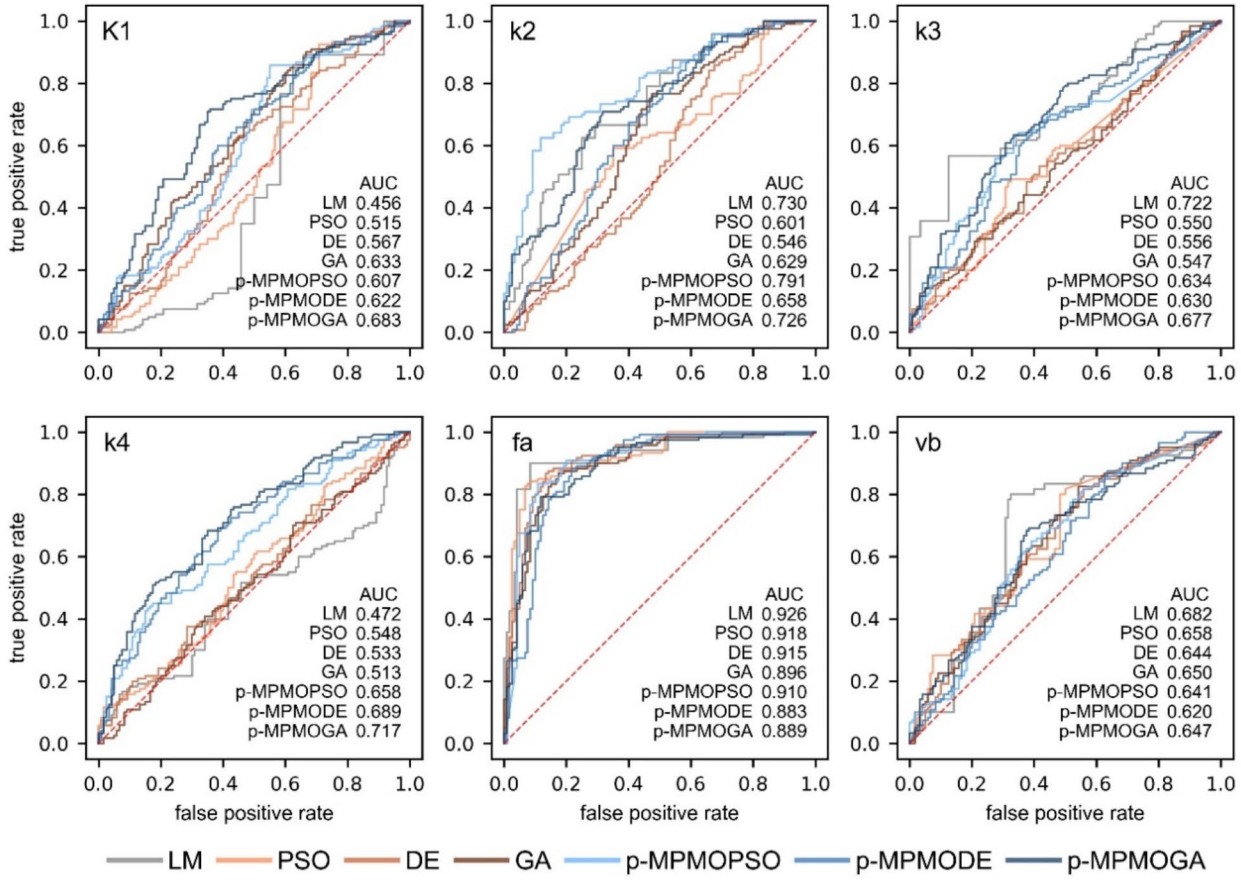

Fig. 4 ROC curve of parameters from all methods

solution space may lead to parameter values that, despite minor errors, lack physiological interpretability. This circumstance may lead to statistically insignificant parameter differences, then failing to yield sufficient clinical diagnostic significance [22]. To address this problem, some studies have used prior information to improve the algorithmic optimization by setting bounds on parameters based on the prior information [19] or setting a parameter with a specific estimated parameter [20]. Nevertheless, these approaches impose excessive restrictions on the parameters, potentially neglecting parameters in other value ranges that could provide an accurate fit. Thus, further research to utilize the prior information based on soft constraints, guiding the algorithm to obtain parameters that are more physiologically reasonable [13, 21–23]. In our study, the guiding role of the prior information is imposed on each individual (parameter point) of the population optimization, while reward mechanisms for physiological characteristics are implemented in the population initialization and objective function. Ultimately, a framework for the multi-population multi-objective optimization algorithm based on the idea of the prior classification is proposed.

In the utilization of prior information, p-MPMO optimization has the following three features: Independent, the subpopulations are independent without information exchange. Each subpopulation works independently, so the mechanism of the method is easy to implement and modify; Adaptive, the number of subpopulations is determined by the number of data categories so that the optimization problem with a wide range of categories can be adapted to the design of multiple subpopulations; Prior-based, the prior information in our approach is the prior result of the parameter estimation, and is involved in the computation of the optimization process in the form of a probability distribution. The prior probability distribution may help to ensure the population retains the parameters' physiological reasonableness while optimizing, however, the fitting remains the main objective in practice. We recommend that the prior probability weights be set to a small value ($\sum_i w_i \leq 0.3$) and the specific prior probability weight of each kinetic parameter needs to be determined according to the prior probability distribution used and the physiological rationality preference on this parameter.

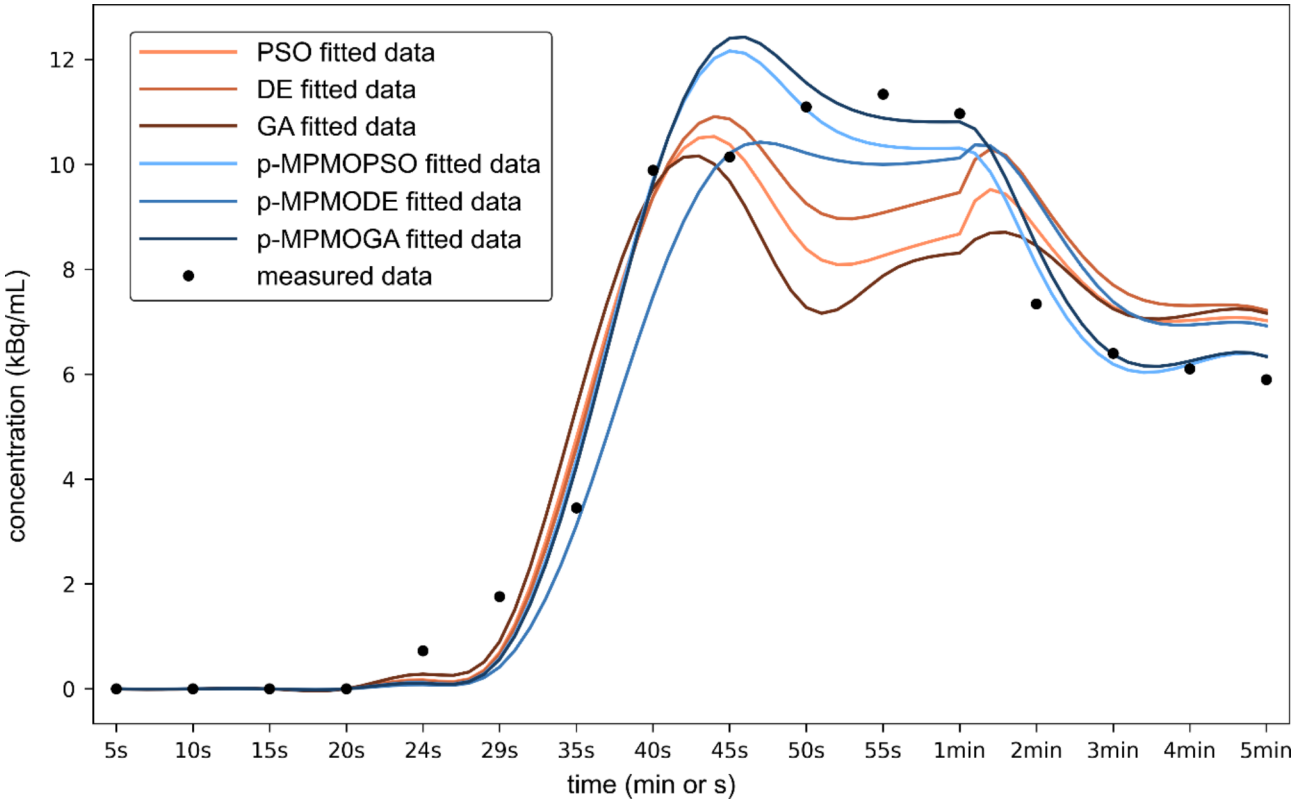

Fig. 5 TACs fitting result

Table 5 The DeLong tests result of several algorithms paired on the same parameter

Parameter	Algorithm 1 (AUC)	Algorithm 2 (AUC)	*P* value	Parameter	Algorithm 1 (AUC)	Algorithm 2 (AUC)	*P* value
k_2	LM (0.730)	p-MPMOPSO (0.791)	0.027	k_3	LM (0.722)	p-MPMOPSO (0.634)	0.009
k_2	LM (0.730)	p-MPMODE (0.658)	0.094	k_3	LM (0.722)	p-MPMODE (0.630)	0.004
k_2	LM (0.730)	p-MPMOGA (0.726)	0.924	k_3	LM (0.722)	p-MPMOGA (0.677)	0.276
f_a	LM (0.926)	p-MPMOPSO (0.910)	0.321	v_b	LM (0.682)	p-MPMOPSO (0.641)	0.257
f_a	LM (0.926)	p-MPMODE (0.883)	0.036	v_b	LM (0.682)	p-MPMODE (0.620)	0.161
f_a	LM (0.926)	p-MPMOGA (0.889)	0.016	v_b	LM (0.682)	p-MPMOGA (0.647)	0.371
f_a	PSO (0.918)	p-MPMOPSO (0.910)	0.580	v_b	PSO (0.658)	p-MPMOPSO (0.641)	0.651
f_a	DE (0.915)	p-MPMODE (0.883)	0.093	v_b	DE (0.644)	p-MPMODE (0.620)	0.573
f_a	GA (0.896)	p-MPMOGA (0.889)	0.704	v_b	GA (0.650)	p-MPMOGA (0.647)	0.937

The p-MPMO optimization was applied with three population algorithms, PSO, DE, and GA. A comparison was made with the LM algorithm and the SPPSO, SPDE, and SPGA. The optimization problem in this study was constructed around tracer kinetic modeling, and each parameter in r-DI3CM was expected to present the physiological significance of Pharmacokinetics in the result. The infusion of liver tissue includes both hepatic artery and portal vein, and the proportion of arterial supply in lesion tissue was higher (70 ~ 80%), while that in healthy liver tissue is lower (20%~30%) [28], the parameter results for all methods in this paper correctly demonstrate this difference. The cellular uptake of ^{18}F-FDG involves its transport across the cell membrane via glucose transporters (Gluts), followed by phosphorylation mediated by hexokinase to produce ^{18}F-FDG-6-phosphate. This metabolic conversion renders it non-metabolizable and amenable to cellular retention. Moreover, phosphatase dephosphorylates ^{18}F-FDG-6-phosphate back to ^{18}F-FDG. Elevated levels of glucose-6-phosphatase are characteristic of the normal liver, leading to the dephosphorylation of ^{18}F-FDG. Consequently, this results in its diminished accumulation within cells and its re-entry into the metabolic cycle [31–34]. Previous studies have shown higher K_1 and k_3 values in kinetic modeling due to a substantial increase in hexokinase activity in malignancies [35], p-MPMOPSO, p-MPMODE, and p-MPMOGA both correctly presented such results and were statistically significant differences in our experimental results. In contrast, the k_4 of dephosphating is

higher than HCC due to greater G6P activity in healthy liver tissue [1], as demonstrated by the three p-MPMO methods. In addition, the differentiation grade of the tumor affects the presentation of some physiological characteristics, such as a well-differentiated tumor may have a similar level of FDG uptake to normal liver tissue [36]. It is not clear but worth to study whether kinetic parmeters function to distinguish the degree of HCC differentiation; unfortunately, this study was not performed because of a small size of the sample.

In ROC analysis, the three p-MPMO optimization algorithms achieved better diagnostic performance than the corresponding single population algorithms. In K_1 and k_4, the three p-MPMO methods achieved significantly better diagnostic performance than the corresponding single population algorithms and the LM algorithm. In k_2 and k_3, the three p-MPMO methods were better than the corresponding single population algorithms, but compared to the LM algorithm in k_2, the p-MPMOPSO was significantly better, the p-MPMOGA was no significant difference, the p-MPMODE was significantly worse, and compared to the LM algorithm in k_3, the three p-MPMO optimization algorithms were significantly worse. This is most likely due to the lack of significant difference in k_2 and k_3 between HCC and normal liver tissue in the distribution of prior parameters shown in Fig. 3. In f_a and v_b, there was no statistically significant difference in diagnostic performance between the seven algorithms, except that p-MPMODE and p-MPMOGA were significantly worse than that of the LM algorithm in f_a. It can be seen that the resulting trend of these two parameters is relatively fixed in parameter estimation practice, and the changes in the algorithm rarely have an impact on estimation.

This study has limitations. First, the acquisition method and quality of the prior information and hepatic dynamic PET data are critical problems. These factors lead to research being hampered by experimental source data. Second, the relationship between kinetic parameters and tumor differentiation grade was not analyzed in a small sample size in this study, and a large sample size research should be further carried out. Another limitation is that the method presented in this paper involves many hyperparameters, and the setting of these parameters relies on subjective judgments, especially the prior weights of each kinetic parameter. Finally, the approach employed in this research adopts a simplistic weighted sum method to perform the multi-objective optimization between the RMSE and prior score. However, this approach may not assure an optimal equilibrium between the two objectives, thus a more effective alternative should be developed in future research.

Conclusions

In this paper, we propose a multi-population multi-objective approach based on the prior information for kinetic parameter estimation in a reversible double-input three-compartment model. The approach achieved ideal performance when combined with the PSO, DE, and GA, and the experimental results demonstrated that these algorithms may present more physiological differences between normal liver tissue and HCC especially according to K_1 and k_4 than conventional methods with the help of the kinetic parameter prior information.

Abbreviations

^{18}F-FDG	18 F fluoro-D-glucose
PET	Positron emission tomography
CT	Computed tomography
p-MPMOO	Prior-based multi-population multi-objective optimization
HCC	Hepatocellular carcinoma
LM algorithm	Levenberg–marquardt algorithm
PSO	Particle swarm optimization
DE	Differential evolution
GA	Genetic algorithm
AUC	Areas under the curve
TKM	Tracer kinetic modeling
TAC	Time-activity curve
NLLS	Nonlinear least squares
OSEM	Ordered subsets expectation maximization
ROIs	Regions of interest
SUVmax	Maximum standardized uptake value
r-DI-3CM	Reversible double-input three-compartment model
RMSE	Root-mean-square error
ROC	Receiver operating characteristic

Acknowledgements

Not applicable.

Author contributions

Yiwei Xiong and Siming Li designed and conducted the research, and also contributed to the writing of the paper. Siming Li was involved in the analysis. Jianfeng He and Shaobo Wang provided critical revisions to the manuscript and oversaw the research. All authors have reviewed and approved the final version of the manuscript.

Funding

This work was sponsored by the National Natural Science Foundation of China (No. 82160347 and 82260355), No. 202102AE090031; The Yunnan Key Laboratory of Smart City in Cyberspace Security (No. 202105AG070010), Ten Thousand People Plan in Yunnan Province (No. YNWR-QNBJ2018-243), and the Basic Research on Application of Joint Special Funding of Science and Technology Department of Yunnan Province-Kunming Medical University (No. 202301AY070001-211).

Data availability

The datasets generated and analyzed during the present study are not accessible to the public due to data security concerns. However, interested parties may request access to these datasets from the corresponding author, subject to reasonable conditions.

Declarations

Ethics approval and consent to participate

This study was conducted in adherence to the principles outlined in the Declaration of Helsinki, and the research protocol received approval from the Ethics Committee of the First People's Hospital of Yunnan Province (No. KHLL2022-KY189). The informed consent of the experimental participants was obtained before the experimental data collection.

Consent for publication
Not applicable.

Competing interests
The authors declare no competing interests.

Author details
[1]Faculty of Information Engineering and Automation, Yunnan Key Laboratory of Artificial Intelligence, Kunming University of Science and Technology, Kunming, Yunnan 650500, China
[2]PET/CT Center, Affiliated Hospital of Kunming University of Science and Technology, First People's Hospital of Yunnan, Kunming 650031, China
[3]School of Physics and Electronic Engineering, Yuxi Normal University, Yuxi 653100, China

Received: 11 January 2024 / Accepted: 16 December 2024
Published online: 24 February 2025

References

1. Keiding S. Bringing physiology into pet of the liver. J Nucl Med. 2012;53(3):425–33. https://doi.org/10.2967/jnumed.111.100214.
2. Gunn RN, Gunn SR, Cunningham VJ. Positron emission tomography compartmental models. J Cereb Blood Flow; Metabolism. 2001;21(6):635–52. https://doi.org/10.1097/00004647-200106000-00002.
3. Huo L, Guo J, Dang Y, et al. Kinetic analysis of dynamic 11 C-acetate PET/CT imaging as a potential method for differentiation of hepatocellular carcinoma and benign liver lesions. Theranostics. 2015;5(4):371–7. https://doi.org/10.7150/thno.10760.
4. Sokoloff L, Reivich M, Kennedy C, et al. The [14c]deoxyglucose method for the measurement of local cerebral glucose utilization: theory, procedure, and normal values in the conscious and anesthetized albino rat. J Neurochem. 1977;28(5):897–916. https://doi.org/10.1111/j.1471-4159.1977.tb10649.x.
5. Graham MM, Muzi M, Spence AM et al. Regional FDG lumped constant in the normal human brain. Physiological imaging of the brain with PET. Published Online 2001:115–20. https://doi.org/10.1016/b978-012285751-5/50020-x
6. Munk OL, Bass L, Roelsgaard K, Bender D, Hansen SB, Keiding S. Liver kinetics of glucose analogs measured in pigs by PET: importance of dual-input blood sampling. J Nucl Med. 2001;42(5):795–801.
7. Brix G, Ziegler SI, Bellemann ME, et al. Quantification of [(18)F]FDG uptake in the normal liver using dynamic PET: impact and modeling of the dual hepatic blood supply. J Nucl Med. 2001;42(8):1265–73.
8. Zanotti-Fregonara P, Chen K, Liow J-S, Fujita M, Innis RB. Image-derived input function for Brain Pet studies: many challenges and few opportunities. J Cereb Blood Flow; Metabolism. 2011;31(10):1986–98. https://doi.org/10.1038/jcbfm.2011.107.
9. Marquardt DW. An algorithm for least-squares estimation of nonlinear parameters. J Soc Ind Appl Math. 1963;11(2):431–41. https://doi.org/10.1137/0111030.
10. Zuo Y, Sarkar S, Corwin MT, Olson K, Badawi RD, Wang G. Structural and practical identifiability of dual-input kinetic modeling in dynamic pet of liver inflammation. Phys Medicine; Biology. 2019;64(17):175023. https://doi.org/10.1088/1361-6560/ab1f29.
11. Wang J, Shao Y, Liu B, et al. Dynamic 18F-FDG PET imaging of liver lesions: evaluation of a two-tissue compartment model with dual blood input function. BMC Med Imaging. 2021;21(1). https://doi.org/10.1186/s12880-021-00623-2.
12. He J, Wang T, Li Y, Deng Y, Wang S. Dynamic chaotic gravitational search algorithm-based kinetic parameter estimation of hepatocellular carcinoma on 18F-FDG PET/CT. BMC Med Imaging. 2022;22(1). https://doi.org/10.1186/s12880-022-00742-4.
13. He J, Li Y, Wang T, Deng Y, Wang S. Kinetic parameter estimation of hepatocellular carcinoma on 18F-FDG PET/CT based on bayesian method. Med Phys. 2022;50(5):2860–71. https://doi.org/10.1002/mp.16139.
14. Kennedy J, Eberhart R. Particle swarm optimization. Proceedings of ICNN'95 - International Conference on Neural Networks. Published online 1995. https://doi.org/10.1109/icnn.1995.488968
15. Storn R, Price K. Differential evolution–a simple and efficient heuristic for global optimization over continuous spaces. J Global Optim. 1997;11(4):341–59. https://doi.org/10.1023/a:1008202821328.
16. Holland JH. Genetic algorithms. Sci Am. 1992;267(1):66–73. http://www.jstor.org/stable/24939139.
17. Sari H, Mingels C, Alberts I et al. First results on kinetic modelling and parametric imaging of dynamic 18 F-FDG datasets from a long axial FOV PET scanner in oncological patients. Eur J Nuclear Med Mol Imaging Published Online 2022:1–13. https://doi.org/10.1007/s00259-021-05623-6
18. Kamasak ME, Bouman CA, Morris ED, Sauer K. Direct reconstruction of kinetic parameter images from dynamic PET data. IEEE Trans Med Imaging. 2005;24(5):636–50. https://doi.org/10.1109/acssc.2003.1292316.
19. O'Sullivan F, Saha A. Use of ridge regression for improved estimation of kinetic constants from PET data. IEEE Trans Med Imaging. 1999;18(2):115–25. https://doi.org/10.1109/42.759111.
20. Bertoldo A, Sparacino G, Cobelli C. Population' approach improves parameter estimation of kinetic models from dynamic PET data. IEEE Trans Med Imaging. 2004;23(3):297–306. https://doi.org/10.1109/tmi.2004.824243.
21. Lin Y, Haldar JP, Li Q, Conti PS, Leahy RM. Sparsity constrained mixture modeling for the estimation of kinetic parameters in dynamic PET. IEEE Trans Med Imaging. 2013;33(1):173–85. https://doi.org/10.1109/tmi.2013.2283229.
22. Ghovvati M, Khayati G, Attar H, Vaziri A. Kinetic parameters estimation of protease production using penalty function method with hybrid genetic algorithm and particle swarm optimization. Biotechnol Biotechnol Equip. 2016;30(2):404–10. https://doi.org/10.1080/13102818.2015.1134279.
23. Kang SK, Seo S, Lee CH, Kim MJ, Kim SJ, Lee JS. Robust nonlinear parameter estimation in tracer kinetic analysis using infinity norm regularization and particle swarm optimization. Physica Med. 2020;72:60–72. https://doi.org/10.1016/j.ejmp.2020.03.013.
24. Huang SC, Phelps ME, Hoffman EJ, Sideris K, Selin CJ, Kuhl DE. Noninvasive determination of local cerebral metabolic rate of glucose in man. Am J Physiology-Endocrinology Metabolism. 1980;238(1):E69–82. https://doi.org/10.1152/ajpendo.1980.238.1.e69.
25. DeLong ER, DeLong DM, Clarke-Pearson DL. Comparing the areas under two or more correlated receiver operating characteristic curves: a nonparametric approach. Biometrics Published Online 1988;837–45. https://doi.org/10.2307/2531595
26. Samimi R, Kamali-Asl A, Geramifar P, van den Hoff J, Rahmim A. Short-duration dynamic FDG PET imaging: optimization and clinical application. Physica Med. 2020;80:193–200. https://doi.org/10.1016/j.ejmp.2020.11.004.
27. Wang S, Wu H, Wang Q, et al. Combined early dynamic 18F-FDG PET/CT and conventional whole-body 18F-FDG PET/CT provide one-stop imaging for detecting hepatocellular carcinoma. Clin Res Hepatol Gastroenterol. 2015;39(3):324–30. https://doi.org/10.1016/j.clinre.2014.10.010.
28. Wang S, Li B, Li P, et al. Feasibility of perfusion and early-uptake 18f-fdg pet/ct in primary hepatocellular carcinoma: a dual-input dual-compartment uptake model. Japanese J Radiol. 2021;39(11):1086–96. https://doi.org/10.1007/s11604-021-01140-6.
29. Wang T, Li B, Shi H, et al. Short-term PET-derived kinetic estimation for the diagnosis of hepatocellular carcinoma: a combination of the maximum-slope method and dual-input three-compartment model. Insights into Imaging. 2023;14(1):1–14. https://doi.org/10.1186/s13244-023-01442-5.
30. Zanotti-Fregonara P, Fadaili EM, Maroy R, et al. Comparison of eight methods for the estimation of the image-derived input function in dynamic [18F]-FDG PET human brain studies. J Cereb Blood Flow Metabolism. 2009;29(11):1825–35. https://doi.org/10.1038/jcbfm.2009.93.
31. Haberkorn U, Ziegler SI, Oberdorfer F, et al. FDG uptake, tumor proliferation and expression of glycolysis associated genes in animal tumor models. Nucl Med Biol. 1994;21(6):827–34. https://doi.org/10.1016/0969-8051(94)90162-7.
32. Paudyal B, Paudyal P, Oriuchi N, Tsushima Y, Nakajima T, Endo K. Clinical implication of glucose transport and metabolism evaluated by 18F-FDG PET in hepatocellular carcinoma. Int J Oncol. 2008;33(5):1047–54. https://doi.org/10.3892/ijo_00000093.
33. Paudyal B, Oriuchi N, Paudyal P, Higuchi T, Nakajima T, Endo K. Expression of glucose transporters and hexokinase II in cholangiocellular carcinoma compared using [18F]-2-fluro-2-deoxy-D-glucose positron emission tomography. Cancer Sci. 2008;99(2):260–6. https://doi.org/10.1111/j.1349-7006.2007.00683.x.
34. Amann T, Maegdefrau U, Hartmann A, et al. GLUT1 expression is increased in hepatocellular carcinoma and promotes tumorigenesis. Am J Pathol. 2009;174(4):1544–52. https://doi.org/10.2353/ajpath.2009.080596.
35. He YX, Guo QY. Clinical applications and advances of positron emission tomography with fluorine-18-fluorodeoxyglucose (18F-FDG) in the diagnosis of liver neoplasms. Postgrad Med J. 2008;84(991):246–51. https://doi.org/10.1136/pgmj.2007.066589.

36. Martins-Filho SN, Paiva C, Azevedo RS, Alves VAF. Histological grading of hepatocellular carcinoma—a systematic review of literature. Front Med. 2017;4:193.

Publisher's note